

## The Impact of Surface Flux Parameterizations on the Modeling of the North Atlantic Ocean

AFONSO M. PAIVA

*COPPE/PEO, Universidade Federal do Rio de Janeiro, Rio de Janeiro, Brazil*

ERIC P. CHASSIGNET

*Rosenstiel School of Marine and Atmospheric Science, University of Miami, Miami, Florida*

(Manuscript received 6 March 2000, in final form 11 October 2000)

### ABSTRACT

The response of an ocean general circulation model to several distinct parameterizations of the surface heat and freshwater fluxes, which differ primarily by their representation of the ocean–atmosphere feedbacks, is investigated in a realistic configuration for the North Atlantic Ocean. The impact of explicitly introducing oceanic information (climatological sea-surface temperature) into the computation of the heat flux through a Haney-type restoring boundary condition, as opposed to the case in which the flux is based on atmosphere-only climatologies and is computed with the full bulk formulation, is considered. The strong similarity between these two approaches is demonstrated, and the sources of possible differences are discussed. When restoring boundary conditions are applied to the surface salinity, however, an unphysical feedback mechanism is being introduced. The model's response to this restoring is contrasted to the response to a flux boundary condition that prescribes the freshwater flux derived from evaporation, precipitation, and river runoff climatologies (and therefore does not allow any feedback), as well as to the more realistic case in terms of the feedback parameterization, in which the dependence of evaporation on the model sea surface temperature is explicitly represented. Limited-area models introduce a further complicating factor for the thermodynamic adjustment, namely the representation of the oceanic heat and freshwater fluxes at the lateral boundaries. The degree to which the model solution is influenced by such fluxes, in combination with the different surface parameterizations, is also assessed. In all cases, the various components of the model's thermodynamic adjustment are considered, and the interdependence between the surface fluxes and the simulated sea surface temperature and surface salinity, their combined effect upon the ventilation of subsurface layers and production of different water masses, and their effect upon the simulated meridional heat and freshwater transports are analyzed.

### 1. Introduction

The ocean can be viewed as a thermodynamic system, the equilibrium of which is determined by the balance between the energy exchanges through the ocean–atmosphere interface, which are unevenly distributed in space and time, and by the internal redistribution of its state variables by the large-scale wind- and thermohaline-driven circulations. The thermodynamic forcing on the ocean surface consists primarily of two components: the heat flux (radiative and turbulent) and the freshwater flux (balance between evaporation and precipitation). These two components induce changes in the sea surface temperature (SST) and sea surface salinity (SSS), respectively, and, when combined, modify the buoyancy of the surface fluid, inducing at times vigorous mixing.

Through this process, properties (temperature and salinity) acquired at the ocean surface are transferred to subsurface and deep layers, distinct water masses are formed, and the thermohaline circulation is induced.

Several numerical studies have been carried out in recent decades to investigate the conditions that determine the present oceanic equilibrium state (the climate) and those that lead to variations from this equilibrium state (the climate variability) [see McWilliams (1996) and Rahmstorf et al. (1996) for reviews]. Traditionally, ocean general circulation models (OGCMs) have relied on restoring surface boundary conditions, which are relatively easy to implement and which prevent long term drifts of the model surface fields. A rich variety of multiple equilibria (Bryan 1986; Marotzke and Willebrand 1991; Moore and Reason 1993; Hughes and Weaver 1996) and of low-frequency oscillatory states (Weaver and Sarachik 1991; Cai et al. 1995) of the overturning circulation have been observed to occur in experiments in which the SSS restoring boundary conditions are replaced by the freshwater flux diagnosed from the

---

*Corresponding author address:* Dr. Eric P. Chassignet, RSMAS/MPO, University of Miami, 4600 Rickenbacker Causeway, Miami, FL 33149-1098.  
E-mail: echassignet@rsmas.miami.edu

model's equilibrium solution. It has been argued, however, that model stability in such cases is strongly dependent upon the timescale of the SSS restoring forcing (Tziperman et al. 1994) and upon the removal of SST anomalies by the strong thermal damping resulting from the assumption (which underlies the restoring approach) of an atmosphere with infinite heat capacity (Zhang et al. 1993; Rahmstorf and Willebrand 1995; Cai 1995; Cai and Chu 1996). Climate-oriented experiments, like the ones mentioned above, require very long integrations, and are therefore generally carried out at very low resolutions and/or with simplified geometries.

Simulations that aim toward a detailed investigation of the various components of the oceanic thermodynamic system under equilibrium forcing are generally designed with realistic configurations and increased resolution, and usually make use of only one (or a few) of the several possible parameterizations of the surface fluxes, the choice of which generally depends upon personal preferences and/or upon the availability of the forcing datasets. This choice, however, can strongly constrain the model solution (Seager et al. 1995) and affect the realism of equilibrium OGCM solutions (Large et al. 1997). Since ocean-only models simplify or eliminate the feedbacks between the ocean and the atmosphere, the ability of an ocean model to appropriately simulate the surface fluxes, and consequently its ability to represent the water mass transformations and transports associated with the thermohaline circulation, is directly dependent upon the parameterization of the surface thermodynamic forcing.

In the present study, an OGCM response to distinct parameterizations of the surface heat and freshwater fluxes, which differ primarily in their representations of the ocean-atmosphere feedbacks, is investigated in a realistic configuration for the North Atlantic Ocean. The various components of the model's thermodynamic adjustment are considered in this investigation, and the interdependence between the surface fluxes and the simulated SST and SSS, their combined effect upon the ventilation of subsurface layers and production of different water masses, and their effect upon the simulated meridional heat and freshwater transports are analyzed. This investigation has also been carried out in order to set the stage for a detailed investigation of atmospheric-forced low-frequency variability in the same model configuration (Paiva and Chassignet 2001, manuscript submitted to *J. Phys. Oceanogr.*).

The paper is organized as follows. The different surface flux parameterizations discussed in this study, and their associated feedback mechanisms, are reviewed in section 2. Details of the model configuration are given in section 3, followed by a brief description of the model adjustment in section 4. The simulated surface fields, meridional heat and freshwater transports, and ventilation of subsurface layers are presented in sections 5, 6, and 7, respectively. The results are then summarized and discussed in section 8.

## 2. Background

This section reviews the surface flux boundary conditions traditionally used in ocean-only models, and introduces the different parameterizations discussed in this paper.

### a. Heat flux

The total downward surface heat flux ( $Q$ ) is a function of the net downward radiation ( $Q_R$ ) and of the latent ( $Q_L$ ) and sensible ( $Q_S$ ) heat fluxes,

$$Q = Q_R - Q_L - Q_S, \quad (1)$$

and can be computed using bulk aerodynamic equations (Bunker 1976; da Silva et al. 1994), with oceanic (SST, hereafter also referred to as  $T$ ) and atmospheric (wind speed, air temperature, specific humidity, . . .) quantities. Several climatological estimates of the total heat flux (hereafter referred to as  $Q_{\text{net}}$ ) have been derived (e.g., Isemer and Hasse 1987; da Silva et al. 1994; Barnier et al. 1995), based on various datasets and on different assumptions regarding the computation of the transfer coefficients used in the bulk parameterizations. Using the climatological estimates of  $Q_{\text{net}}$  to force an OGCM generally results in unrealistic model SST, which then become inconsistent with the imposed surface flux (Barnier et al. 1995), since this flux is computed from observed SST. In order to minimize this inconsistency, a feedback between the model and the prescribed atmosphere can be introduced by replacing the observed SST (hereafter  $T_o$ ) by the model SST (hereafter  $T_m$ ) in the formulation of  $Q$  [Eq. (1)], which is then computed during the simulation.

This model SST feedback on the surface heat flux is often simplified by linearizing Eq. (1) (Haney 1971), the so-called Haney-type boundary condition,

$$Q_H = \lambda(T^* - T_m), \quad (2)$$

in which the apparent equilibrium temperature  $T^*$  and the coupling coefficient  $\lambda$  are space and time dependent fields, derived from either atmospheric data only (Han 1984) or from atmospheric and oceanic data (Oberhuber 1988; da Silva et al. 1994; Barnier et al. 1995). In the first case, the linearization is performed around an atmospheric temperature  $T_a$ , with

$$\lambda = \left. \frac{dQ}{dT} \right|_{T=T_a}, \quad T^* = T_a + \frac{Q(T = T_a)}{\lambda}, \quad (3)$$

while in the second case the linearization is around an oceanic temperature  $T_o$ , with

$$\lambda = \left. \frac{dQ}{dT} \right|_{T=T_o}, \quad T^* = T_o + \frac{Q(T = T_o)}{\lambda}. \quad (4)$$

One advantage of the Haney-type boundary condition linearized around SST [Eq. (4)] is that the climatological estimate of  $Q_{\text{net}}$  chosen to force the model is recovered

when the model reproduces  $T_o$  (note that  $Q$  evaluated at  $T_o$  is equivalent to  $Q_{\text{net}}$ ). SST can also be observed with reasonable accuracy from satellites, whereas the surface air temperature cannot.

The above linearization has often been invoked as a physical justification for the more pragmatic approach, commonly used in ocean modeling until recently, of substituting the climatological SST ( $T_o$ ) for  $T^*$  in Eq. (2), while considering constant values for  $\lambda$  (Seager et al. 1995). This approach, however, which represents a simple restoring of  $T$  toward  $T_o$ , has several shortcomings (Killworth et al. 2000), since (i) it leads to a time lag between the model and climatological SST, which is inversely proportional to the restoring strength (Pierce 1996); (ii) it results in zero flux when the model temperature agrees with climatology ( $T_m = T_o$ ); and (iii) it results in a heat flux that is only weakly correlated to observations (Chu et al. 1998). These limitations are a consequence of replacing  $T^*$  with  $T_o$  in Eq. (2) and not of the linearization itself.

The linearization makes explicit the restoring to climatology implicitly present when using the bulk formulas to compute the heat flux in ocean models. To the extent that the above linearizations are good approximations of Eq. (1), forcing the model with a heat flux computed with the bulk formulation is analogous to forcing the model with Haney-type boundary conditions. It is this characteristic of the bulk formulations (when computed with a prescribed atmosphere) that prevents the model SST from diverging strongly from observations. In all these approaches, the model SST is forced toward an equilibrium temperature (explicitly represented by  $T^*$  in the Haney formulation).

One could argue that using climatological oceanic SST in Eq. (4) introduces the answer into the problem, unduly restraining the model solution in contrast to fluxes obtained from atmospheric climatologies only [Eqs. (1) or (3)]. However, as shown in Fig. 1, the observed air temperature is very strongly correlated to SST. This means that a forcing of the model SST toward  $T_o$  as explicitly done in Eq. (2) is almost equivalent to a forcing of the model SST toward  $T_o$  as in Eq. (4) (Seager et al. 1995). All formulations (bulk formulas or Haney-type), therefore, carry oceanic information within themselves.

#### b. Freshwater flux

The freshwater flux into the ocean ( $F$ ) is given by the difference between precipitation ( $P$ ) and evaporation ( $E$ ) rates, plus the contribution from river runoff ( $R$ ),

$$F = P - E + R. \quad (5)$$

Climatological evaporation rates are computed from the bulk formula for latent heat (divided by the latent heat of vaporization), with oceanographic SST and atmospheric observations. Precipitation can be derived from ship-based observations, in which case it is esti-

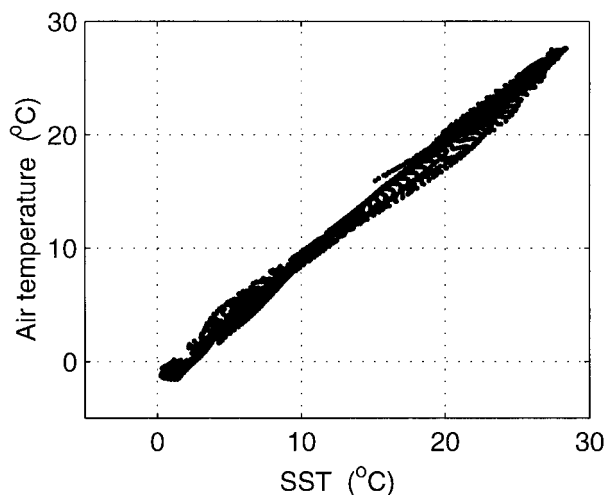


FIG. 1. Scatter diagram of climatological air temperature vs climatological SST (from the COADS climatology).

mated from present weather reports (Schmitt et al. 1989) or from satellite observations (Spencer 1993).

The use of the climatological freshwater flux to force a numerical model does not constrain the evolution of SSS, which is then free to evolve according to the model internal dynamics. In contrast to the analogous approach described for the heat flux, this approach does not create any inconsistency between the model SSS and the surface freshwater flux since the flux  $F$  is independent of SSS. However, it does not take into account the feedback exerted by the model SST upon precipitation and evaporation.

The SST feedback on precipitation can only be estimated in a coupled ocean–atmosphere model that includes moisture transport (Hughes and Weaver 1996), a topic that is outside the scope of the present study. The feedback on evaporation, however, can be computed during the simulation, by replacing the observational ( $T_o$ ) by the model ( $T_m$ ) SST in the bulk parameterization of latent heat,

$$F = P - E(T_m) + R. \quad (6)$$

The importance of the evaporation feedback can be evaluated from climatology by computing the rate of change of evaporation with respect to the observed SST ( $dE/dT|_{T_o}$ ). Typical values for the North Atlantic are on the order of  $10^{-8} \text{ m s}^{-1} \text{ deg}^{-1}$  (Fig. 2a). For differences between  $T_m$  and  $T_o$  on the order of  $1^\circ\text{C}$  (characteristic of model results), changes in evaporation due to the SST feedback are of the same order of magnitude as the climatological evaporation itself [ $\sim 1$  to  $8 (\times 10^{-8} \text{ m s}^{-1})$  in the North Atlantic, as seen in Fig. 2b].

In order to minimize the deviation of the model SSS from observation, a different approach has been widely used in OGCMs (e.g., Bryan and Lewis 1979; Holland and Bryan 1994; New et al. 1995; Chassignet et al. 1996; DYNAMO 1997; Willebrand et al. 2000), in

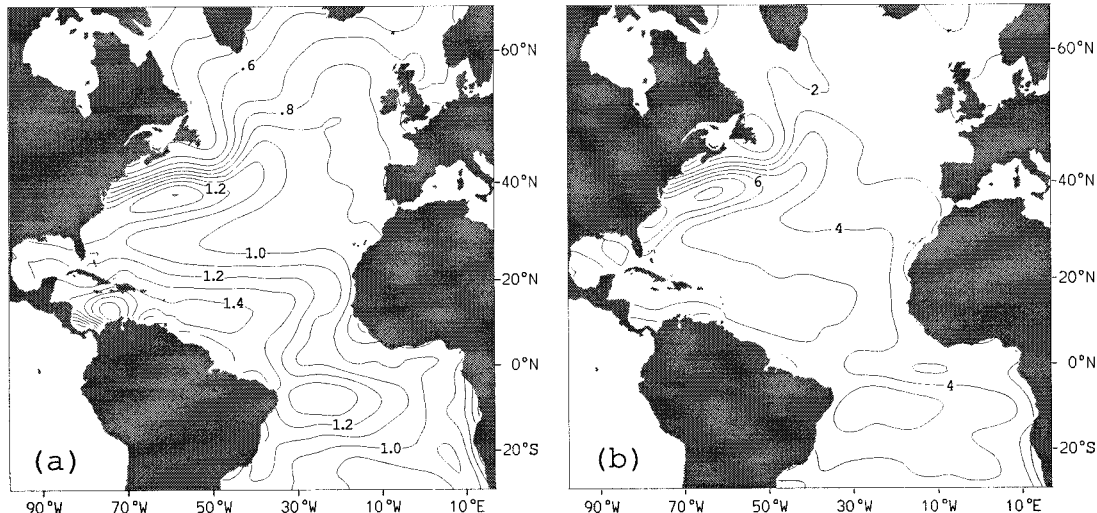


FIG. 2. Coupling coefficient  $dE/dT|_{T_o}$ , expressing the strength of the model temperature feedback on the surface freshwater flux (units in  $10^{-8} \text{ m s}^{-1} \text{ }^\circ\text{C}^{-1}$ ), and (b) the annual average evaporation rate, both derived from the COADS climatology (units in  $10^{-8} \text{ m s}^{-1}$ ).

which the model surface salinity ( $S_m$ ) is restored toward climatological values ( $S_o$ ), implying a freshwater flux represented by

$$F = \lambda_S(S_o - S_m). \quad (7)$$

The coefficient  $\lambda_S$  is usually a constant, and is chosen to be equivalent to a restoring timescale on the order of 30–60 days, analogous to the typical values obtained from the heat flux climatologies. However, in contrast to the Haney formulation for the heat flux, there is no physical justification for the feedback exerted by SSS upon the freshwater flux in Eq. (7). The representation of the freshwater flux as in Eq. (7) has been advocated by many authors primarily on the basis of the lack of reliable datasets for the surface freshwater flux over the oceans, in particular for precipitation (Holland and Bryan 1994). Furthermore, the shortcomings of this formulation are the same as the ones discussed for the heat flux formulation when a simple restoring toward SST is used, that is, a time lag in the model response, zero flux for  $S_m = S_o$ , and small correlation to observed fluxes.

### 3. Model configuration

The ocean numerical model is the Miami Isopycnic Coordinate Ocean Model (Bleck et al. 1992; Bleck and Chassignet 1994), configured with realistic topography and stratification. The computational domain is the North and equatorial Atlantic Ocean basin from 28°S to 65°N, including the Caribbean Sea and the Gulf of Mexico. The bottom topography is derived from a digital terrain dataset with 5° latitude–longitude resolution (ETOPO5) by averaging the topographic data located in each grid box. Open ocean boundaries are treated as closed, but are outfitted with 3° buffer zones in which

temperature ( $T$ ) and salinity ( $S$ ) are linearly relaxed toward their seasonally varying climatological values (Levitus 1982). These buffer zones restore the  $T$  and  $S$  fields to climatology in order to approximately recover the vertical shear of the currents through geostrophic adjustment.

The horizontal grid is defined on a Mercator projection with resolution given by  $1^\circ \times 1^\circ \cos(\phi)$ , where  $\phi$  is the latitude. The vertical density structure is represented by 15 isopycnic layers ( $\sigma_\theta$  values of 24.70, 25.28, 25.27, 26.18, 26.52, 26.80, 27.03, 27.22, 27.38, 27.52, 27.64, 27.74, 27.82, 27.88, and 27.92), topped by a dynamically active Kraus–Turner surface mixed layer. The vertical discretization was chosen to provide maximum resolution in the upper part of the ocean.

The experiments discussed in this paper differ by the parameterization of the thermodynamic forcing and by the presence or absence of the relaxation conditions in the lateral buffer zones. The experiments are summarized in Table 1 and are described below. The model's response to the surface heat flux formulation is investigated for (a) the bulk formulation [Eq. (1) computed with  $T_m$  as in Bleck et al. (1992)], and (b) the linearization around  $T_o$  [Eqs. (2) and (4)]. In the bulk formulation, the transfer coefficients for latent and sensible heat fluxes are constant and equal to  $1.2 \times 10^{-3}$  (equivalent to neutral atmospheric stability). The model's response to the surface freshwater forcing is investigated for (i) a prescribed climatological flux [Eq. (5)], (ii) a prescribed climatological precipitation (including river runoff) with evaporation computed as a function of the model temperature [Eq. (6)], and (iii) a restoration of the model SSS to climatology [Eq. (7)]. In all cases, the freshwater flux is implemented as a virtual salt flux.

The coupling coefficient for the Haney-type boundary condition [Eq. (4)] is a space and time dependent field

TABLE 1. Summary of model experiments. The experiment acronyms indicate that (i) the heat flux ( $Q$ ) is a function either of atmospheric climatologies only ( $Q_A$ ), or of atmospheric and ocean climatologies ( $Q_O$ ), and (ii) that the freshwater flux  $F$  is either derived from climatology for both precipitation (including river runoff) and evaporation ( $Q_{P-E}$ ), from climatology for precipitation, but with an SST model-dependent evaporation ( $F_{P-E(T)}$ ), or from a relaxation of the model toward climatological SSS ( $F_{RS}$ ). The bulk formulation [Eq. (1)] is computed with  $T_m$  (model SST) as in Bleck et al. (1992) using the COADS climatology (da Silva et al. 1994). The same climatology is used to derive the apparent equilibrium temperature  $T^*$  and the coupling coefficient  $\lambda$  [Eq. (4)]. The asterisks refer to experiments without buffer zone relaxation.

Expt	Heat flux	Freshwater flux	Buffer zone relaxation
$Q_A F_{P-E}$	Bulk formulation	$P - E + R$	Yes
$Q_O F_{P-E}$	$\lambda(T^* - T_m)$	$P - E + R$	Yes
$Q_O F_{P-E(T)}$	$\lambda(T^* - T_m)$	$P - E(T) + R$	Yes
$Q_O F_{RS}$	$\lambda(T^* - T_m)$	$\lambda_S(S_o - S_m)$	Yes
$Q_O F_{P-E}^*$	$\lambda(T^* - T_m)$	$P - E + R$	No
$Q_O F_{RS}^*$	$\lambda(T^* - T_m)$	$\lambda_S(S_o - S_m)$	No

derived from observations. In the freshwater forcing, however, the restoring coefficient is a constant, chosen to correspond to a restoring timescale of 50 days for a mixed layer depth of 35 m, consistent with the range

of values generally used in depth coordinate models (Chassignet et al. 1996). All surface climatologies are based on the Comprehensive Ocean–Atmosphere Data Set (COADS) (da Silva et al. 1994), with the exception of SSS, which is derived from Levitus (1982), and river runoff, which is based on Perry et al. (1996). The freshwater river runoffs are added to the precipitation field; freshwater input from sea-ice melt is not prescribed, but is implicit in the experiments with surface salinity restoring. All simulations are initialized from the Levitus (1982) climatology and spun up from rest for a total of 20 years.

#### 4. Model adjustment during the spinup phase

The geostrophic adjustment to the initial climatological mass field leads to a rapid development of the wind- and thermohaline-driven circulation, and the model annual average total kinetic energy and surface fields change little after the first 10 years of simulation. The only exception to this behavior is experiment  $Q_O F_{P-E}^*$ , which will be discussed in more detail in section 6. After 20 years of integration, the deep layers are still undergoing a slow adjustment related (i) to the heat and salt (freshwater) flux into the model interior domain,

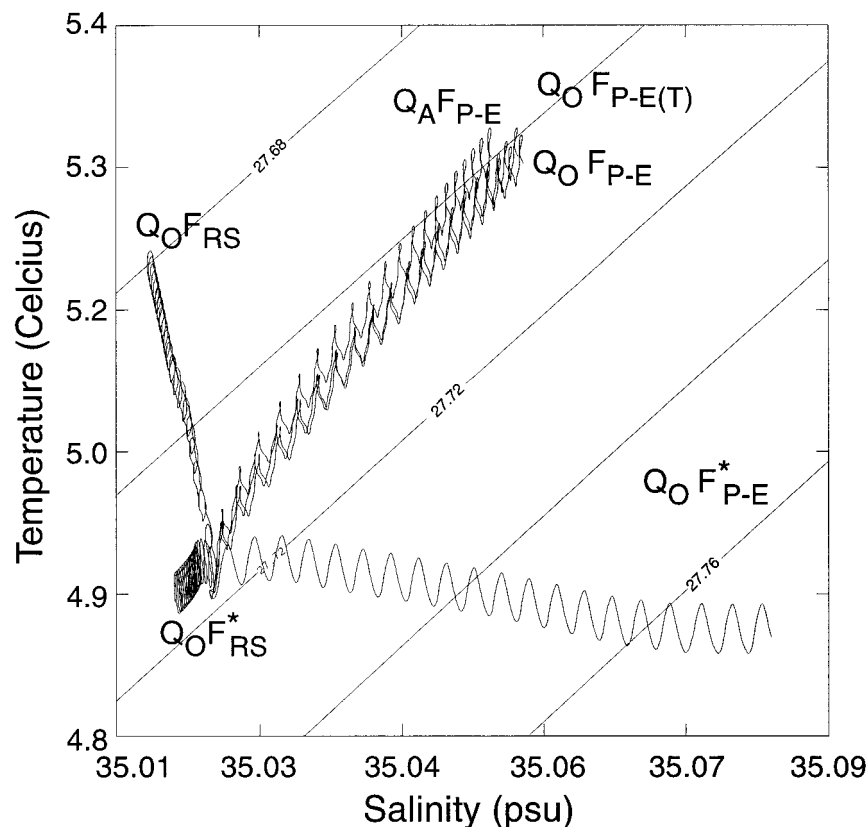


FIG. 3. Temperature–salinity diagram, showing the time evolution of the total domain mass-weighted temperature and salinity, for the model experiments listed in Table 1. All experiments were initialized with the same mass field derived from Levitus (1982).

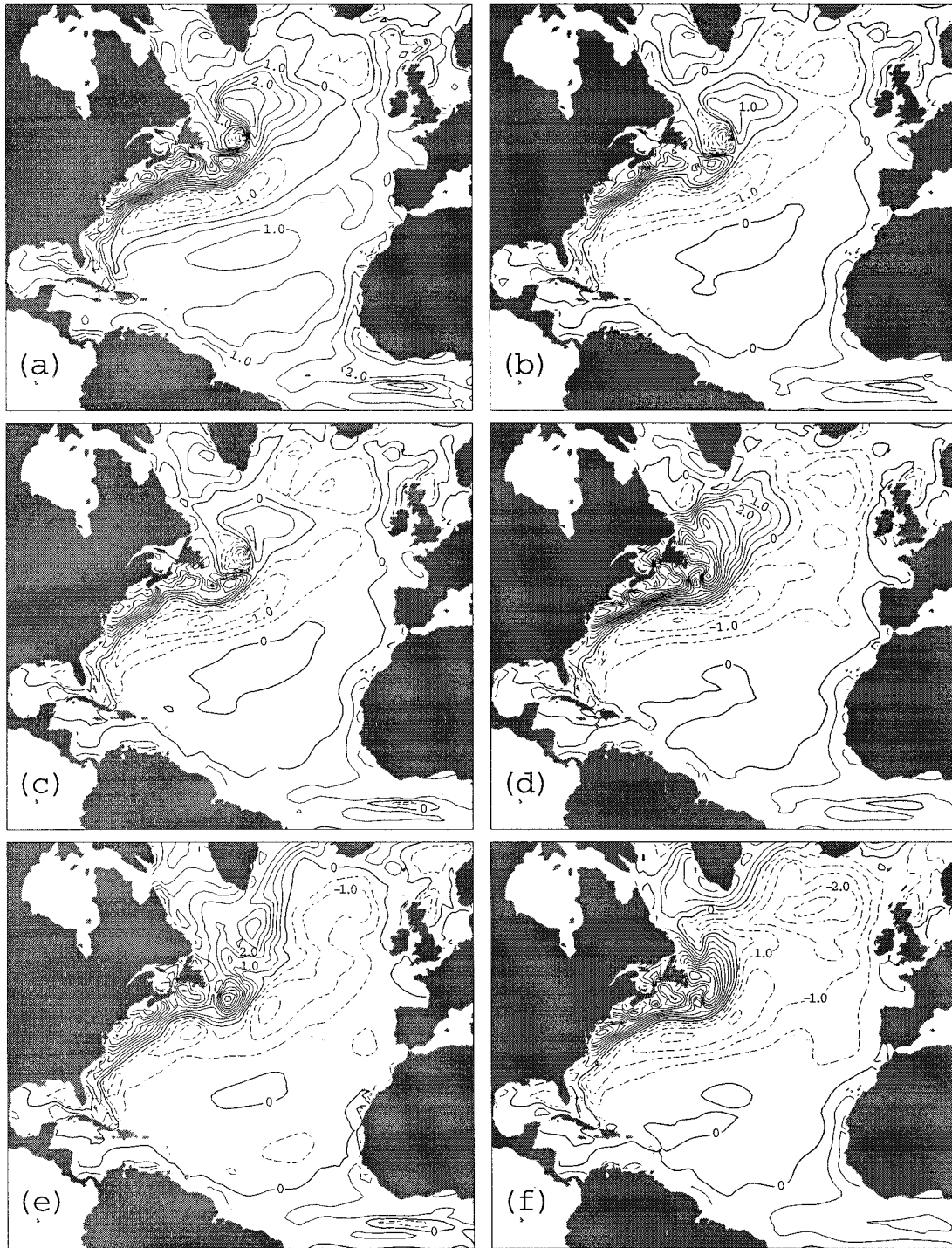


FIG. 4. Difference between model and COADS SST climatology (contour interval of 0.5°C): Expts (a)  $Q_A F_{P-E}$ , (b)  $Q_O F_{P-E(T)}$ , (c)  $Q_O F_{P-E}$ , (d)  $Q_O F_{RS}$ , (e)  $Q_O F_{P-E}^*$  and (f)  $Q_O F_{RS}^*$ .

which is associated with the diabatic transformations occurring within the buffer zones, and (ii) to the interior diapycnal mixing (Chassignet et al. 1996; Paiva et al. 2000).

The time evolution of the domain-averaged temper-

ature and salinity is shown for all experiments in the  $T-S$  phase diagram of Fig. 3 as a proxy for the changes in total heat and salt content during the simulations. Four different characteristic behaviors can be observed, reflecting the impact of both the surface and the lateral

boundary forcing. The average temperature decreases in the experiments without relaxation to climatology in the buffer zones (expts  $Q_O F_{P-E}^*$  and  $Q_O F_{RS}^*$ ) in response to the net surface heat loss to the atmosphere over the model domain. With relaxation in the buffer zones, however, there is a lateral convergence of heat into the domain (Paiva et al. 2000), and the average temperature increases during the simulations in experiments  $Q_A F_{P-E}$ ,  $Q_O F_{P-E}$ ,  $Q_O F_{P-E(T)}$ , and  $Q_O F_{RS}$ . The total heat content in the model does not depend strongly upon the formulation of the surface heat flux, as seen by contrasting experiments  $Q_A F_{P-E}$  (bulk formulas) and  $Q_O F_{P-E}$  (Haney boundary conditions). The warming trend is weaker, however, with restoring to surface salinity (expt  $Q_O F_{RS}$ ) than with flux boundary conditions.

Changes in the average salinity result primarily from the parameterization of the surface freshwater flux. With the restoring conditions on surface salinity, the cases both with and without buffer zone relaxation (expts  $Q_O F_{RS}$  and  $Q_O F_{RS}^*$ ) show a decrease in the total salt content. This implies a net freshwater flux into the ocean, indicating that the model SSSs are greater than the climatological values [see Eq. (7)]. The lateral freshwater divergence at the edges of the buffer zones is very small in both cases, as discussed in section 6. The freshwater flux climatology, however, indicates a net loss over the model domain, with an excess of evaporation over precipitation plus river runoff of  $\sim 0.5$  Sv ( $\text{Sv} \equiv 10^6 \text{ m}^3 \text{ s}^{-1}$ ), and the average salinity increases accordingly in the remaining experiments. The less accentuated increase in the average salinity in experiments  $Q_A F_{P-E}$ ,  $Q_O F_{P-E}$ , and  $Q_O F_{P-E(T)}$ , when contrasted to experiment  $Q_O F_{P-E}^*$ , is a consequence of lateral freshwater convergence provided by the buffer zones, which partially balances the surface loss. The model is not significantly sensitive to the more realistic parameterization of the surface flux in experiment  $Q_O F_{P-E(T)}$ , which includes the SST feedback to evaporation, when contrasted to the imposition of the climatological flux in experiment  $Q_O F_{P-E}$ , and the increase in average salinity follows a similar curve in both cases.

## 5. Surface fields

The simulated surface circulation is characterized by broad and stable currents, typical of the viscous solutions obtained with medium resolution, representing the wind-driven gyres of the equatorial, subtropical, and subpolar regions (Chassignet et al. 1996). The direct effect of the surface flux boundary conditions is to modify the model surface properties. In the following, the relationship between the simulated SST and the surface heat flux, and between the simulated SSS and the surface freshwater flux, are investigated. The model surface climatologies presented in this section were computed using the results of the last year of integration.

### a. SST and heat flux

The differences between the model and the COADS SST climatology are shown in Fig. 4, for all experiments. For clarity, only the North and equatorial Atlantic regions are shown in the figure, and the following discussion is confined to those regions. Features common to all experiments are (i) the higher equatorial temperature in the model, indicating weak upwelling; (ii) the two bands of higher and lower temperature, associated with the northward shifting of the model Gulf Stream; and (iii) moderate temperature differences in a large region in the interior subtropical gyre.

Larger differences between model and climatological SST are observed in experiment  $Q_A F_{P-E}$  (Fig. 4a) than in experiment  $Q_O F_{P-E}$  (Fig. 4c). The simulated SSTs in experiment  $Q_A F_{P-E}$  are warmer than in experiment  $Q_O F_{P-E}$  by as much as  $1^\circ$ – $1.5^\circ\text{C}$  in the subtropical and equatorial regions, and more along the Gulf Stream. The bulk formulation used in experiment  $Q_A F_{P-E}$  implies a stronger heating of the ocean than does the linearized form used in experiment  $Q_O F_{P-E}$ , for the same value of SST. This is true, for instance, when  $T_m = T_o$ , in which case the climatological surface heat loss by the ocean within the model domain estimated with the model bulk formulas is lower than that provided by the  $Q_{\text{net}}$  climatology. The different estimates of  $Q_{\text{net}}$  reflect the assumptions made in the model bulk formulas for practical reasons (i.e., constant instead of stability-dependent transfer coefficients, climatological instead of real-time atmospheric parameters) as well as the fine tuning performed by da Silva et al. (1994) to ensure that, over the entire ocean, the outgoing heat flux balances the incoming heat flux.

Despite the differences in SST, the resulting annually averaged heat flux in both experiments is similar over a large portion of the model domain (Figs. 5a,b). Comparison with the climatological heat flux presented in Fig. 5c also reveals that the model SST feedback can be of the same order of magnitude as the climatological flux itself. Large variations from climatology occur along the southern flank of the Gulf Stream, where subtropical and subpolar mode waters are formed, with possible impact upon the ventilation of the subtropical gyre. The inclusion of the SST feedback on the freshwater flux does not lead to significant differences from the case with prescribed evaporation (compare expt  $Q_O F_{P-E(T)}$  in Fig. 4b to expt  $Q_O F_{P-E}$  in Fig. 4c). The same is true over most of the domain (Fig. 4d) for the case of the freshwater flux based on the restoring of surface salinity to climatology (expt  $Q_O F_{RS}$ ). In this case, however, a stronger warming is observed in the Grand Banks region, which results from a weaker Labrador Current and a stronger Gulf Stream extension.

### b. SSS and freshwater flux

The differences between the model results and the Levitus SSS climatology are shown in Fig. 6, for all

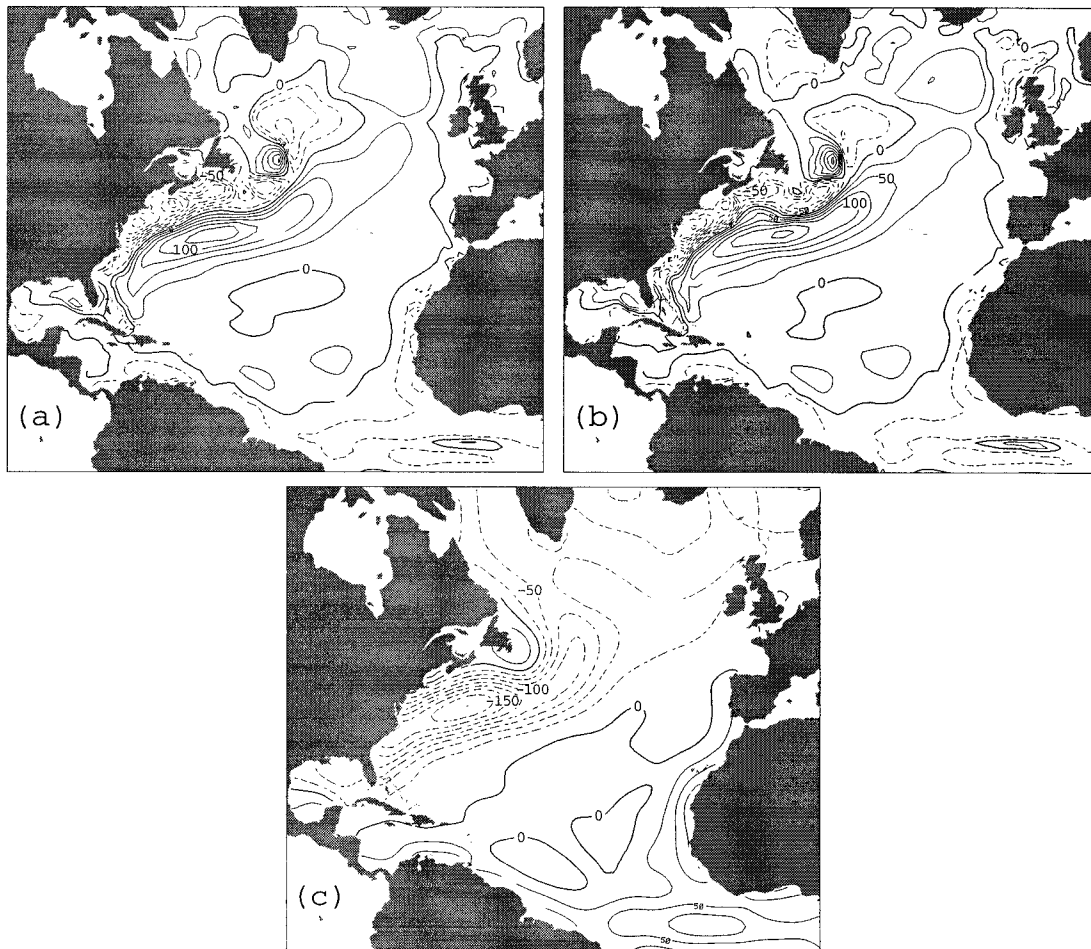


FIG. 5. Difference between model and COADS annual net heat flux (contour interval of  $25 \text{ W m}^{-2}$ ) for expts (a)  $Q_A F_{P-E}$  and (b)  $Q_O F_{P-E}$ . The COADS annual climatology is presented in (c).

experiments. In the experiments with imposed surface freshwater flux, the simulated SSS is higher than observations over most of the domain. The high SSS values near the Antilles reflect a progressive westward displacement via advection of the subtropics SSS maximum during the first 10 years of the simulation. The large differences at the east coast of North America are associated primarily with advection along the overshooting Gulf Stream. Reasonable agreement between the model and observations is found primarily in the central subtropical gyre and at high latitudes. In the latter region, the excess of precipitation over evaporation (Fig. 7c) and the relaxation to surface salinity in the northern buffer zone counteract the salinity increase observed in the rest of the domain.

The inclusion of the temperature feedback on the freshwater flux [expt  $Q_O F_{P-E(T)}$ , Fig. 6b] does not lead to significant changes in the SSS when contrasted to the previous cases in which the climatological flux is prescribed (expts  $Q_A F_{P-E}$  and  $Q_O F_{P-E}$ ). This holds despite the fact that this feedback leads to a surface freshwater flux in experiment  $Q_O F_{P-E(T)}$  that differs from clima-

tology by values on the same order of magnitude as the climatological flux itself (compare Figs. 7a and 7c), in particular in the equatorial and the Gulf Stream regions. In a sense, the inclusion of the temperature feedback upon the freshwater flux could be prejudicial to the simulation of SSS in regions that exhibit higher than observed SSS and SST since higher SST enhances the evaporation. These differences between the simulated and observed SSS and SST, however, occur primarily in regions of strong oceanic advection in which the impact of the surface fluxes is minimized.

In the case of imposed surface freshwater flux but no lateral relaxation in the buffer zones (expt  $Q_O F_{P-E}^*$ ), the SSS increases in the entire subpolar region, in particular in the Labrador Sea (Fig. 6e). The same is true for SST, as seen in Fig. 4e. These increases, resulting from the accumulation at the northern boundary of salt and heat advected by the North Atlantic Current, illustrate the importance of the buffer zones not only for simulating the overturning circulation, but also for producing property transformations that account for the horizontal advection of these properties through the boundaries of

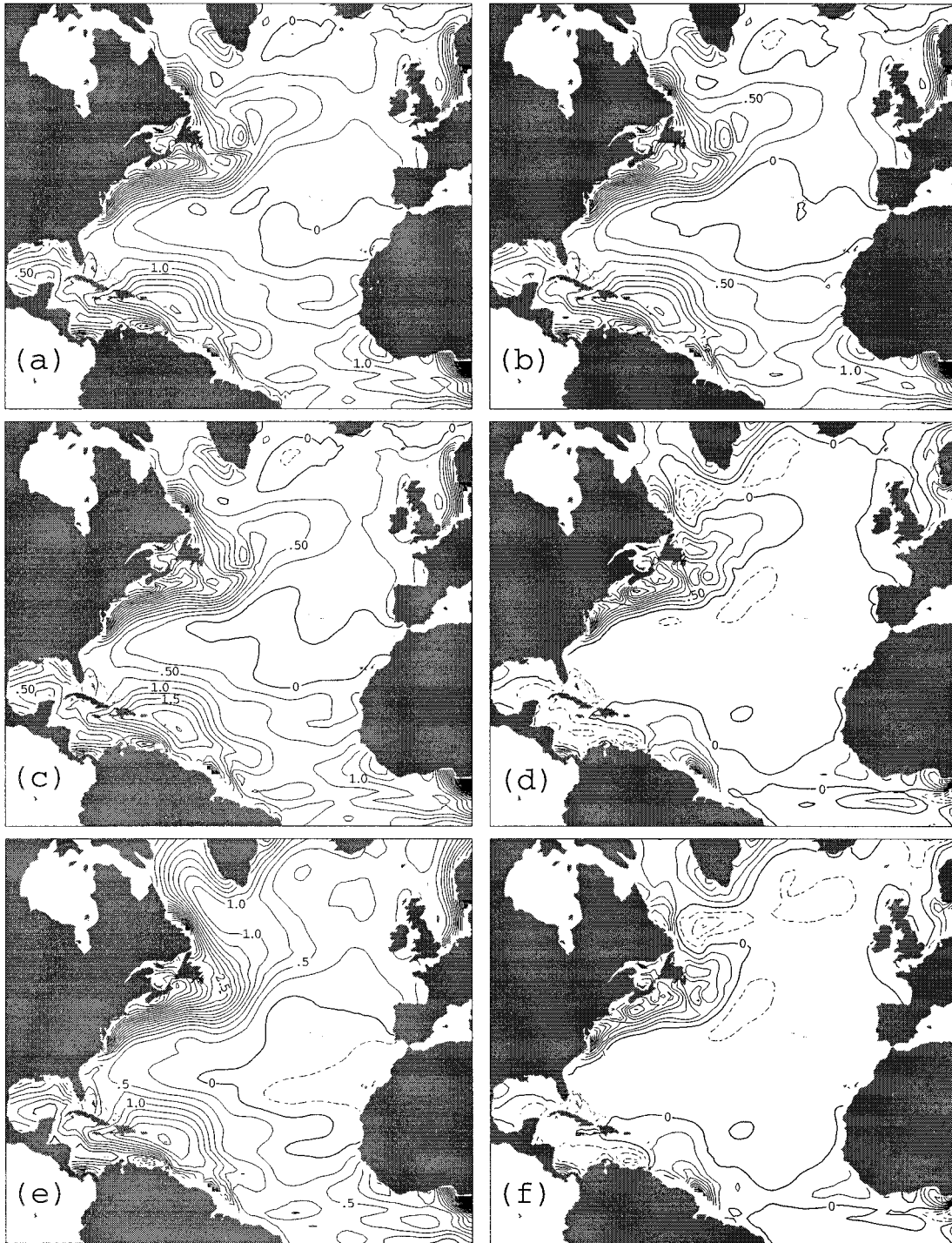


FIG. 6. Difference between model and Levitus (1982) SSS climatology (contour interval of 0.25 psu): Expts (a)  $Q_A F_{P-E}$ , (b)  $Q_O F_{P-E(T)}$ , (c)  $Q_O F_{P-E}$ , (d)  $Q_O F_{RS}$ , (e)  $Q_O F_{P-E}^*$ , and (f)  $Q_O F_{RS}^*$ .

the model domain, eventually balancing the surface freshwater and heat fluxes. In  $Q_O F_{RS}^*$ , the accumulation of salt is prevented by the surface restoring force. In the experiments with surface freshwater flux, fluid particles can undergo unrealistic salinity modifications as

they are advected since (i) the modeled velocity fields differ from observations in magnitude and location and (ii) the uncertainties in the  $P - E$  field are large.

The best overall agreement between observed and modeled SSS occurs, as expected, in the case in which

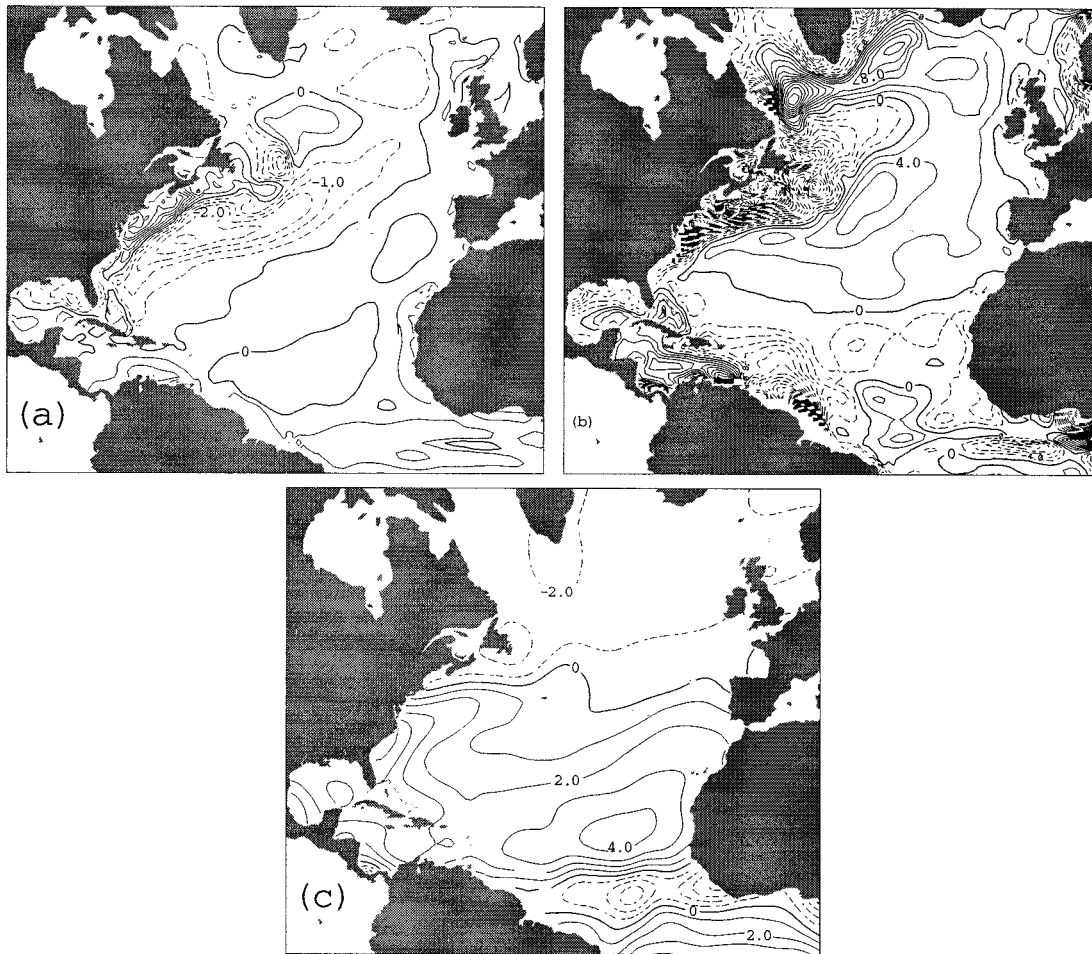


FIG. 7. Difference between model and COADS annual net freshwater flux climatology for expts (a)  $Q_O F_{P-E(T)}$  (contour interval  $0.5 \times 10^{-8} \text{ m s}^{-1}$ ) and (b)  $Q_O F_{RS}$  (contour interval  $2 \times 10^{-8} \text{ m s}^{-1}$ ). The COADS freshwater flux annual climatology (contour interval  $1 \times 10^{-8} \text{ m s}^{-1}$ ) is presented in (c).

the model SSS is restored to climatology (expt  $Q_O F_{RS}$ , Fig. 6d). The correlation between model and observed fluxes, however, is very low, and the differences between them can be one or two orders of magnitude larger than the observed flux itself (compare Figs. 7b and 7c).

## 6. Meridional mass, heat, and freshwater transport

The surface distributions of heat and freshwater fluxes and the meridional heat and freshwater oceanic transports are strongly coupled, and in an equilibrium state the divergence of the meridional transports necessarily balances the zonally integrated surface fluxes. In an ocean model, therefore, the development of the meridional transports is strongly constrained by the degree toward which the ocean state influences the surface fluxes, which is dependent upon the feedback parameterization in the surface forcing. The observed differences between the spatial patterns of surface heat and freshwater fluxes (Figs. 5c and 7c), and between the latitudinal

variation in the meridional transports of heat and freshwater (e.g., Macdonald and Wunsch 1996; Wijffels et al. 1992), suggest that different oceanic mechanisms may be involved in generating each of these transports. In this section, a description of the simulated meridional overturning circulation (MOC) is provided, followed by a comparison between the meridional heat and freshwater transports that result from the diverse surface flux parameterizations. The relative contributions of the MOC and of the wind-driven gyres to the generation of oceanic transports is then investigated.

### a. The overturning circulation

The meridional overturning streamfunctions in experiments  $Q_O F_{P-E}$  (with linearized heat flux and prescribed freshwater flux) and  $Q_O F_{RS}$  (with linearized heat flux and relaxation of SSS to climatology) are shown in density space in Fig. 8, superimposed on the zonally averaged temperature and salinity for each case. The model results are not greatly dependent upon the heat

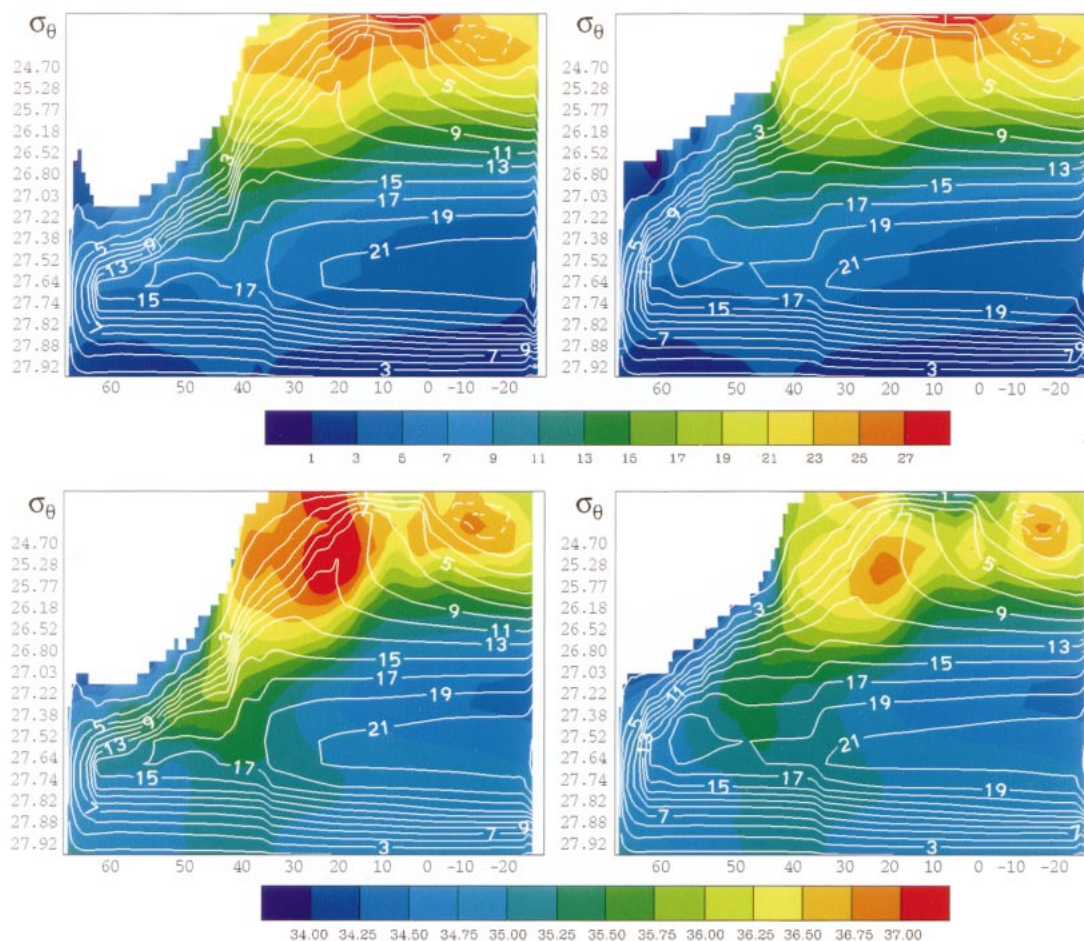


FIG. 8. Meridional overturning streamfunction for expt  $Q_oF_{p-e}$  (left) and expt  $Q_oF_{rs}$ , (right), superimposed on the model zonal-averaged temperature (upper) and salinity (lower). Contour interval of 2 Sv for positive streamfunctions (solid lines) and 0.5 Sv for negative streamfunctions (dashed lines).

flux formulation or upon the temperature feedback on evaporation, and only minor differences are observed between experiments  $Q_oF_{p-e}$  and  $Q_oF_{p-e(T)}$  (not shown) and experiment  $Q_oF_{p-e}$  (Fig. 8, left panels). In these three cases with freshwater flux boundary conditions, denser surface water is transported in the upper branch of the overturning circulation in the subpolar region, reflecting the model tendency to enhance SSS at high latitudes, as discussed in section 5. In the experiment with SSS restoring (expt  $Q_oF_{rs}$ , Fig. 8, right panels), the transport streamfunction magnitude is also similar to that obtained in the experiments with freshwater flux boundary conditions. In all cases,  $\sim 16$ – $17$  Sv circulate through the entire basin, interacting with both the northern and southern buffer zones. This component of the overturning streamfunction is associated primarily with the southward flow of the relatively cold North Atlantic Deep Water in the deep western boundary current, and with the warm return flow in the surface and subsurface layers. The magnitude is in good agreement with observations (Schmitz and McCartney 1993).

When the buffer zone relaxation is shut off in ex-

periment  $Q_oF_{rs}^*$ , the resulting overturning cell is very weak (Fig. 9, right panels), corresponding primarily to the subtropical Ekman cells and to water mass transformations taking place in the Labrador Sea. In an analogous experiment, but with the imposed climatological surface freshwater flux (expt  $Q_oF_{p-e}^*$ , Fig. 9, left panels), however, a strong overturning cell evolves and intensifies during the integration. This cell develops completely in the interior domain, and is driven by convection in the western subpolar gyre (northward of  $\sim 50^\circ\text{N}$ ). With no constraints imposed upon the surface salinity, either in the interior domain or in the buffer zones, the salt transported northward through the North Atlantic Current accumulates in the northern latitudes (Fig. 6e), increasing the mixed layer density and triggering strong deep convection. A tongue of high salinity water can be seen in this case in Fig. 9 (lower-left panel), extending from the subtropics into the subpolar region, and penetrating from the surface into the deep ocean as well.

The salt-driven MOC observed in experiment  $Q_oF_{p-e}^*$  occurs in the opposite sense from the halocline

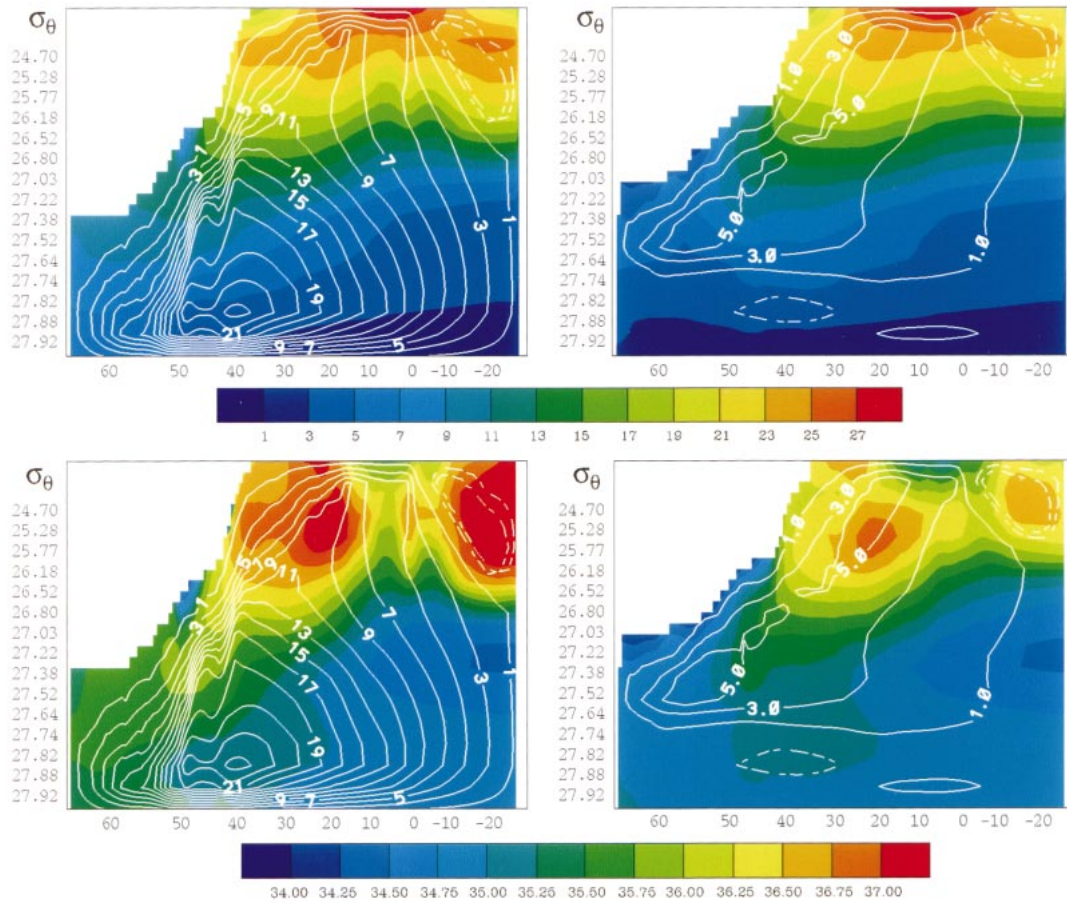


FIG. 9. Meridional overturning streamfunction for expt  $Q_O F_{P-E}^*$  (left) and expt  $Q_O F_{RS}^*$  (right), superimposed on the model zonal-averaged temperature (upper) and salinity (lower). Contour interval of 2 Sv for positive streamfunctions (solid lines) and 0.5 Sv for negative streamfunctions (dashed lines).

catastrophe described by Bryan (1986), in which freshening at high latitudes interrupts convection, reducing, and eventually shutting off, the MOC. A positive feedback mechanism operates in both cases, with the enhanced (reduced) MOC increasing (decreasing) the advection of salt by the North Atlantic Current to high latitudes. A negative feedback also exists in reality in these cases, with the enhanced (reduced) MOC increasing (decreasing) the northward heat advection and, consequently, reducing (enhancing) convection. However, the restoring of the model SST to climatology, explicitly or implicitly represented in the surface heat flux formulations, prevents such a feedback from fully operating in the present simulations.

*b. Heat and freshwater transports*

In the present model configuration, realistic meridional heat and freshwater transports are achieved only when temperature and salinity relaxation toward climatological values are prescribed in the buffer zones. These buffer zones represent processes taking place outside the model domain, such as the production of dense

water in the Greenland–Iceland–Norwegian seas, as well as the subsequent entrainment of upper-layer waters that occurs below the Greenland–Iceland–Scotland ridge. The meridional heat transport is shown in Fig. 10a, for all experiments incorporating the lateral forcing (expts  $Q_A F_{P-E}$ ,  $Q_O F_{P-E}$ ,  $Q_O F_{P-E(T)}$ , and  $Q_O F_{RS}$ ). Also shown for comparison is a residual computation based on the COADS climatology (thick line), which represents the oceanic heat advection necessary to balance the surface heat flux at each latitude. Since such a computation provides only the shape of the transport curve, a nonarbitrary integration constant was added to establish the absolute values by assuming the transport at 24°N to be the 1.2 PW estimated by Hall and Bryden (1982), based on hydrography. Also shown are the inverse computation values of Macdonald and Wunsch (1996). The transports of heat are very similar for all experiments shown, except in the high latitudes of the subpolar gyre where a stronger oceanic convergence of heat is observed in experiment  $Q_O F_{RS}$ . The model results are in good agreement with observations in all cases, particularly in the Northern Hemisphere.

The meridional freshwater transport is shown in Fig.

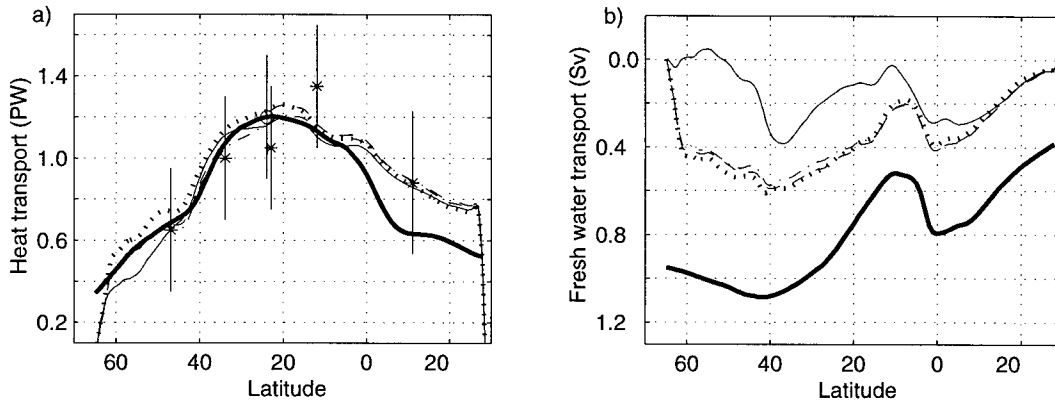


FIG. 10. Meridional heat (a) and freshwater (b) transports in expts  $Q_A F_{P-E}$  (dotted),  $Q_O F_{P-E}$  (dashed),  $Q_O F_{P-E(T)}$  (dashed-dotted), and  $Q_O F_{RS}$  (thin solid). The thick line represents the transports necessary to balance the climatological surface fluxes (see text for details). The circle is the meridional heat transport estimate from Hall and Bryden (1982), and the stars are values from the inverse computation of Macdonald and Wunsch (1996), both based on observations. The vertical lines are error bar estimates.

10b, for experiments  $Q_A F_{P-E}$ ,  $Q_O F_{P-E}$ ,  $Q_O F_{P-E(T)}$ , and  $Q_O F_{RS}$ . In reality, the surface freshwater flux is balanced by an oceanic horizontal divergence of mass. In the model, the surface freshwater flux is replaced by a virtual salt flux (see section 3), and the total mass flux through a zonal section is zero. In that case, the oceanic meridional freshwater flux ( $F_M$ ) can be diagnosed from the meridional salt flux by

$$F_M = \frac{-1}{S_{\text{ref}}} \langle v S_m \rangle, \quad (8)$$

in which  $S_{\text{ref}}$  is a reference salinity,  $S_m$  the model salinity at each grid point,  $v$  the meridional component of the velocity vector, and angle brackets denote the area integral over a zonal section (McCann et al. 1994). Also shown in Fig. 10b is the meridional transport necessary to balance the COADS climatological surface freshwater flux plus the river runoff (thick line), which closely follows the transport derived by integrating the Baumgartner and Reichel (1975) climatology. The freshwater transport through the Bering Straits is included in the observations, following Wijffels et al. (1992), but not in the model. This accounts in part for the bias between the model results and the observations.

In the experiments with surface flux boundary conditions (expts  $Q_A F_{P-E}$  and  $Q_O F_{P-E}$ ), the model solutions converge toward the imposed climatological flux. The meridional freshwater transport in the experiment with restoring surface boundary conditions (expt  $Q_O F_{RS}$ ), however, differs significantly from that in the cases with surface flux boundary conditions, particularly at mid and high latitudes where the freshwater divergence is close to zero. A near zero divergence in the Atlantic was also found by McCann et al. (1994), when analyzing the freshwater transport in global simulations under restoring surface boundary conditions for salinity, and was attributed to an inadequate simulation of Antarctic Intermediate Water (AAIW), resulting in an increased

northward salt transport. In experiment  $Q_O F_{RS}$ , however, the AAIW is well represented (Fig. 8), and the best agreement between model and observed fluxes is found at lower latitudes. At high latitudes, the higher (in relation to observations) oceanic freshwater divergence is a consequence of the intense surface freshwater flux (Fig. 7b) induced by the overshooting Gulf Stream.

### c. The overturning and gyre contributions

In order to gain an understanding of the processes that determine the meridional heat and freshwater (salt) transports, the relative contributions of the overturning circulation and of the wind-driven gyres is investigated for experiment  $Q_O F_{P-E}$ . While there is no rigorous way to separate the overturning and gyre components from the total transport (Rahmstorf 1996), one estimate (Bryan and Lewis 1979; Tziperman and Bryan 1993; Böning and Herrmann 1994) is given by

$$\langle v\theta \rangle = \langle \bar{v}\bar{\theta} + \overline{v'\theta'} \rangle, \quad (9)$$

in which the angle brackets stands for the zonal area integral, the overbar denotes a zonal average, and the primes represent the departure from the average. The variable  $\theta$  stands for  $\rho C_p T$  for the heat transport ( $\rho$  is the water density and  $C_p$  the specific heat at constant pressure) and for  $-S_m/S_{\text{ref}}$  for the freshwater transport. The overturning component is estimated in the first term on the right-hand side of Eq. (9) as the product of the zonally averaged velocity by the zonally averaged temperature or salinity. The horizontal correlations in the second term on the right-hand side of Eq. (9) correspond to the transport due to the wind-driven gyres.

The total heat transport, and the MOC and gyre contributions, are shown in Fig. 11 (upper panel). The results agree with the notion that the meridional heat transport is related primarily to the overturning circulation, which transports cold deep water southward and warm

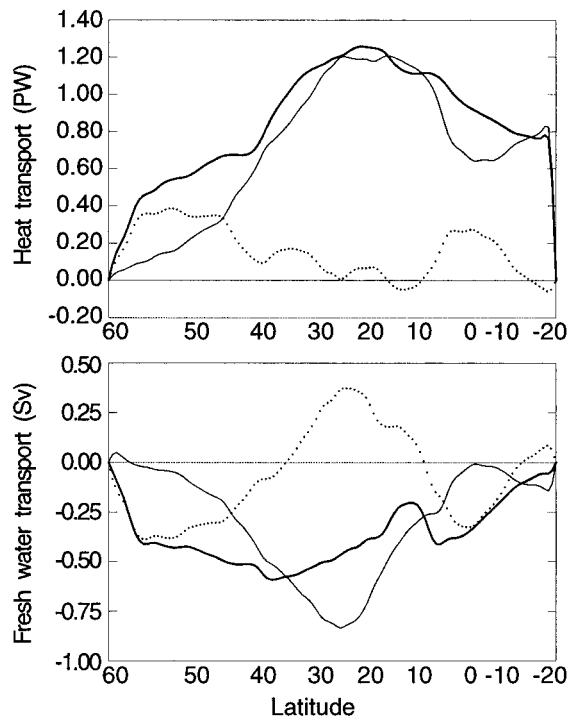


FIG. 11. Meridional heat (upper) and fresh water (lower) transports in expt  $Q_o F_{p-e}$ , divided into total transport (thick solid lines), overturning contribution (thin solid lines), and gyre contribution (dotted lines). See text for details on the computation.

surface and subsurface waters northward (Fig. 8, upper panels), while the horizontal temperature distribution is fairly zonal (Smith et al. 2000). The decrease in transport at low latitudes is related to the opposing effects on the surface poleward heat transport by the Ekman cells in the two hemispheres. The gyre component is relatively important at high latitudes, where the temperature contrast between the upper and the deep ocean is relatively low and the zonal contrast between the warm North Atlantic Current and the cold Labrador Current is relatively high.

The total freshwater transport, plus the MOC and gyre contributions, are shown in Fig. 11 (lower panel). The MOC component transports freshwater primarily southward over the entire domain, in the same sense as the total transport deduced from observations (Fig. 10b). Like the meridional heat transport, this component is a maximum at midlatitudes (near 25°N), where the overturning strength and the salinity contrast between the upper and deep ocean are strong, and decreases accordingly toward high latitudes. In contrast to the heat transport, however, at low latitudes the MOC component of the freshwater flux is very weak. In the South Atlantic, this is due in part to the opposing effect of the surface Ekman cells. To a large extent, however, the reduced freshwater transport at low latitudes arises from the nonmonotonic variation of salinity with depth, and

to the presence of a salinity minimum at middepths, corresponding to the AAIW (Fig. 8, lower panels).

When compared to the total transport (Fig. 10b), the divergence of the MOC component in experiment  $Q_o F_{p-e}$  is stronger in the subpolar gyre, and is of the opposite sign in the northern part of the subtropical gyre (Fig. 11, lower panel), meaning that the overturning circulation removes more freshwater from these regions than that which is supplied by the observed surface flux. In contrast to the meridional heat transport, the meridional freshwater transport is determined to a large extent by the contribution of the wind-driven gyres. In the subtropics, this transport is northward, and reflects the southward advection of high salinity water in the central subtropical gyre. In the subpolar gyre, the weak oceanic freshwater divergence results from the combination of the MOC component with a strong southward freshwater transport by the gyre (Fig. 11, lower panel).

## 7. Mode water formation

In section 5 and 6, the model's response to the surface fluxes was investigated in terms of the degree to which these fluxes constrain the representation of surface properties and meridional transports, two of the most commonly diagnosed results in ocean models. In this section, the resulting ventilation of subsurface layers, which provides the link between the ocean surface and the circulation and property distributions in the deep ocean, is examined.

At midlatitudes, the ventilation of the thermocline is accomplished by subduction, driven by the combined effects of Ekman pumping and geostrophic flow through the base of the late winter mixed layer (Marshall et al. 1993; Williams et al. 1995). Observations show that subduction occurs preferentially in certain density ranges, leading to the formation of relatively thick layers with homogenized properties, or mode waters (McCartney and Talley 1982). In the present simulations, the subtropical gyre thermocline is ventilated primarily by layers 6 ( $\sigma_\theta = 26.52$ ) through 9 ( $\sigma_\theta = 27.22$ ), which outcrop into the winter mixed layer along a line that runs approximately from south of Cape Hatteras, in the western Atlantic, to southern England in the eastern basin. The ventilation process in the model is illustrated in Fig. 12, which shows closed contours defining the region where a particular layer thickness is greater than 200 m in March of the last year of simulation, representing water that has irreversibly left the mixed layer (New et al. 1995; Chassignet et al. 1996). Denser layers outcrop to the northeast, following the increase in mixed layer density in this direction. The ventilation pattern is very similar in experiments  $Q_o F_{p-e}$  (Fig. 12a) and  $Q_A F_{p-e}$  (Fig. 12b), which differ only by the surface heat flux formulation. The slight northeastward displacement of the subduction lenses in the latter experiment, when contrasted to that of the former, reflects the warmer, and consequently lighter, subtropical gyre simulated in ex-

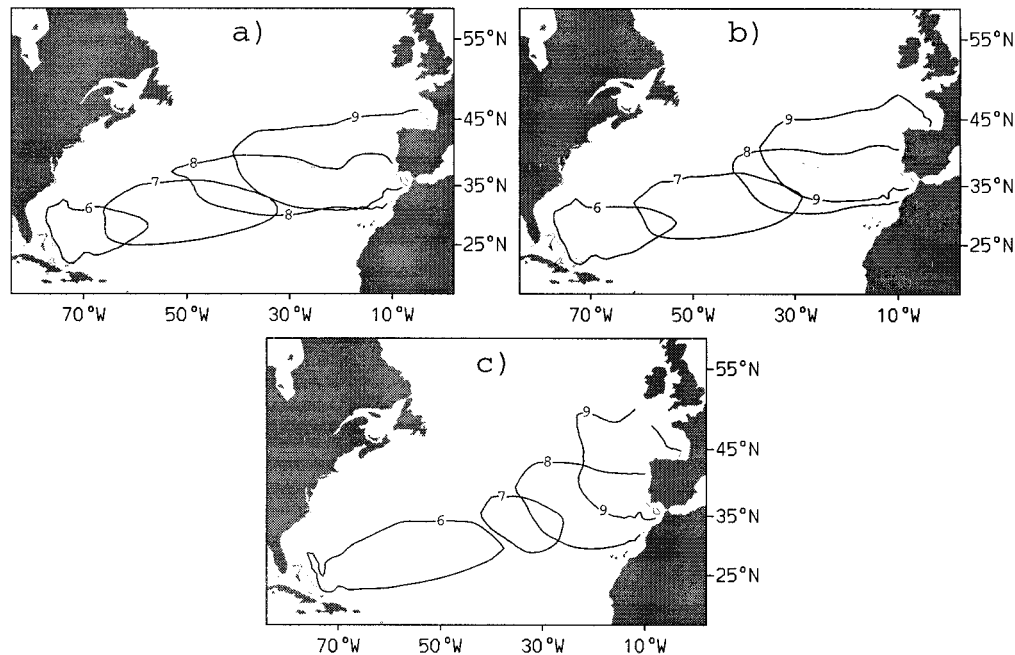


FIG. 12. Area (denoted by solid contours) in which a model layer thickness exceeds 200 m in the subtropical gyre, for layers 6 ( $\sigma_\theta = 26.52$ ), 7 ( $\sigma_\theta = 26.80$ ), 8 ( $\sigma_\theta = 27.03$ ), and 9 ( $\sigma_\theta = 27.22$ ), in Mar of year 20. (a) Expt  $Q_O F_{P-E}$ , (b) expt  $Q_A F_{P-E}$ , and (c) expt  $Q_O F_{RS}$ .

periment  $Q_O F_{P-E}$  (see section 5). The ventilation pattern in experiment  $Q_O F_{RS}$  with SSS restoring (Fig. 12c) differs substantially from that of experiments  $Q_O F_{P-E}$  (Fig. 12a) and  $Q_A F_{P-E}$  (Fig. 12b). The overall fresher and lighter subtropical gyre simulated in experiment  $Q_O F_{RS}$  (see section 5) leads to an eastward displacement of the outcropping region, with the denser layers (7–9) being ventilated primarily in the eastern basin, and layer 6 occupying most of the Sargasso Sea.

A complementary view of the mode water formation in the model is given by the volumetric  $T$ – $S$  diagram computed from the last year of simulation, shown in Figs. 13a–c, which is compared to the volumetric  $T$ – $S$  diagram computed from the Levitus (1982) annual climatology, shown in Fig. 13d. The subtropical and subpolar mode waters are represented in this figure by the large volumes concentrated in small areas lying between temperatures of  $\sim 7^\circ$ – $18^\circ\text{C}$  and salinities of  $\sim 35.0$ – $36.5$  psu, the characteristic range for the North Atlantic Central Water. The bias toward higher SSS observed in the experiments forced with the climatological freshwater flux (Figs. 6a–c), and without any constraints on the simulated SSS, is seen to propagate into the thermocline, leading to a displacement in the  $T$ – $S$  diagram of the mode waters along isopycnals toward higher salinities, and consequently higher temperatures (Figs. 13a,b). Note, however, that the southwestward displacement of the outcropping line due to the increase in mixed layer density is followed by a vertical upward migration of the isopycnals, and consequently by a cooling of the thermocline. This scenario of warming along isopycnals

and cooling at constant depth levels is analogous to that described by New and Bleck (1995). However, in the present case, it is driven primarily by the increase in mixed layer salinity, whereas in their experiments it was a consequence of surface cooling. In the SSS restoring case (Fig. 13c), on the contrary, the subtropical mode water is somewhat fresher, and therefore cooler, and the thermocline is warmer at constant depth levels. Subpolar mode waters at intermediate densities ( $\sigma_\theta = 26.80$  and  $27.03$ ) compare well with climatology in this case, but the denser modes (temperatures less than  $\sim 12^\circ\text{C}$ ), which ventilate the eastern part of the subtropical gyre and the subpolar gyre, have their volume substantially reduced.

The densest mode water created within the model domain is Labrador Sea Water (LSW), which appears in the lower part of the  $T$ – $S$  diagram (Fig. 13) as a large volume of relatively cold and fresh water. LSW is formed by deep convection in the central Labrador Sea, which reaches depths of  $\sim 1000$  m, with typical temperatures in the range  $3.3^\circ$ – $3.4^\circ\text{C}$ , salinities of  $\sim 34.84$ – $34.89$  psu, and  $\sigma_\theta \sim 27.76$ – $27.78$  (Talley and McCartney 1982). In the model, layer 13 ( $\sigma_\theta = 27.74$ ) has a density closest to observed LSW. In the present configuration, the water mass formation in the Labrador Sea proved to be very sensitive to the parameterization of the surface fluxes, and differs significantly among the experiments. These differences are associated primarily with the simulated late winter surface density (a function of the SST and SSS fields), which, in a convective regime, determines to a large extent the volume of water

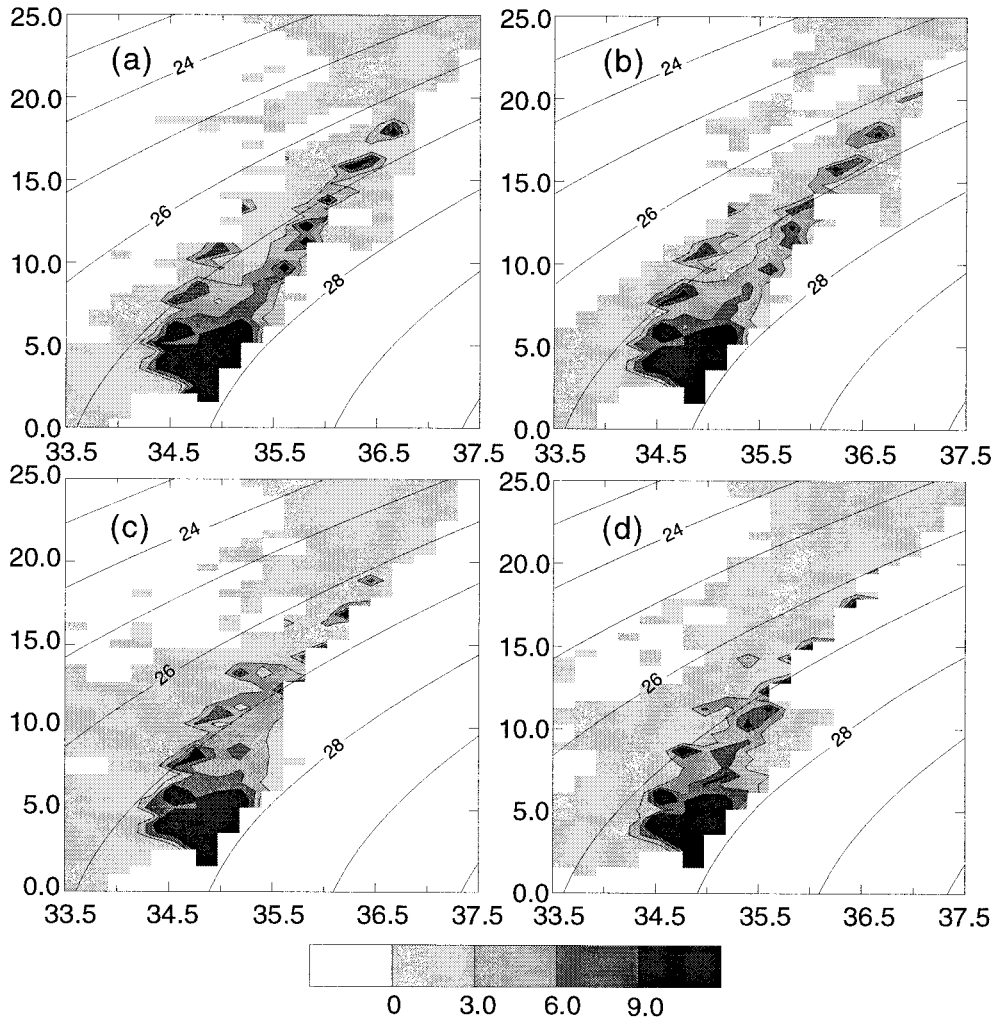


FIG. 13. Volumetric  $T$ - $S$  diagram for (a) expt  $Q_O F_{P-E}$ , (b) expt  $Q_A F_{P-E}$ , (c) expt  $Q_O F_{RS}$ , and (d) Levitus (1982) climatology. Contour Interval in  $10^{14} \text{ m}^3$ .

that is transferred from the mixed layer to each of the model's isopycnic layers.

The time evolution of the simulated layer structure in the central Labrador Sea is shown in Fig. 14. Water with characteristics similar to LSW is initially produced in experiment  $Q_O F_{P-E}$  (Fig. 14a), with the mixed layer ventilating primarily layer 13. By the end of the simulation, however, the slight warming ( $T \sim 3.5^\circ\text{C}$ ) and freshening ( $S \sim 34.76$ ) of the late winter surface layer (not shown) lead to the formation of lighter mode waters in the central Labrador Sea, with both layers 12 ( $\sigma_\theta = 27.64$ ) and 13 ( $\sigma_\theta = 27.74$ ) being ventilated. The surface freshening is attributed to a stronger than observed spreading of freshwater from the Labrador Current, which normally supplies fresh surface water to the central Labrador Sea (Lazier 1973; Pickart 1992); this spreading results from the broad surface currents that are simulated with the present highly diffusive medium resolution configuration. In experiment  $Q_A F_{P-E}$ , with the bulk formulation for the heat flux, the simulation of

a slightly warmer ( $T \sim 3.7^\circ\text{C}$ ) and fresher ( $S \sim 34.74$ ) winter mixed layer reduces significantly the ventilation of layer 13, and a lighter mode water ( $\sigma_\theta = 27.64$ ) is formed in the Labrador Sea (Fig. 14b).

In an apparently paradoxical result, the lowest and most atypical winter SSS ( $\sim 34.25$ ) in the central Labrador Sea was simulated in the experiment with SSS restoring conditions (expt  $Q_O F_{RS}$ ). The simulated freshening of the surface layer leads to a shift from a regime with deep convection in the initial five years of integration, to one in which convection is restricted to the upper 500 m (Fig. 14c). In this situation, the LSW core ( $\sigma_\theta = 27.74$  in the model) is totally isolated from the surface mixed layer, and salinity in the LSW core increases to  $\sim 34.9$  psu due to horizontal mixing with water from the Irminger Sea. This result is similar in many aspects to the interruption of convection observed in the 1960s (Talley and McCartney 1982; Dickson et al. 1996), during the period in which the Great Salinity Anomaly, which originated in the Greenland Sea, oc-

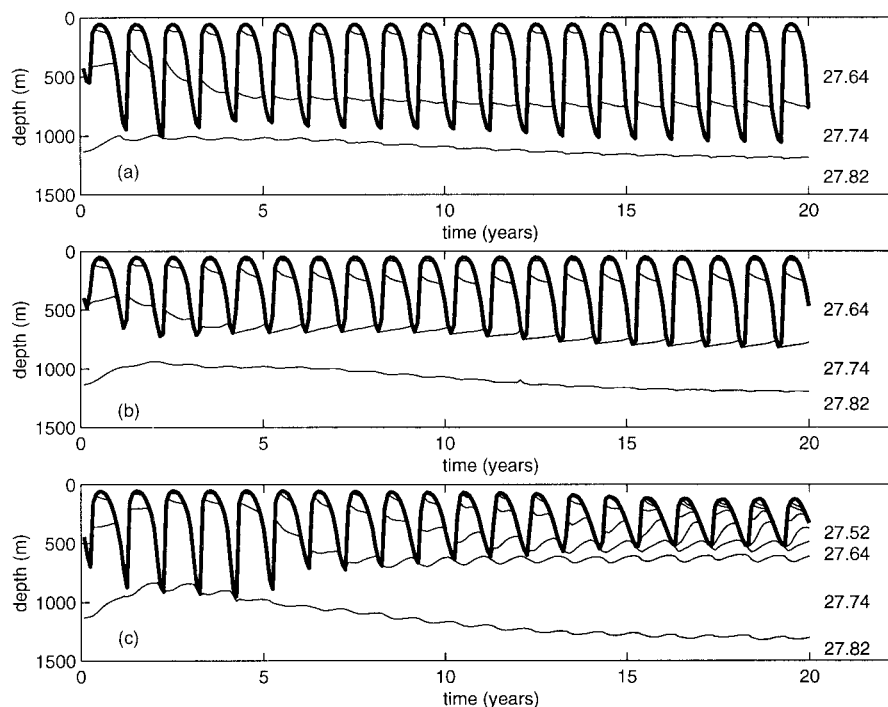


FIG. 14. Time evolution of layer interfaces in the central Labrador Sea (averaged within  $56^{\circ}$ – $52^{\circ}$ N,  $50^{\circ}$ – $52^{\circ}$ W), for expts (a)  $Q_O F_{P-E}$ , (b)  $Q_A F_{P-E}$ , and (c)  $Q_O F_{RS}$ . The thick line is the base of the mixed layer. The numbers to the right indicate the  $\sigma_{\theta}$  values of each model layer.

cupied the Labrador Sea. In the model, however, the surface freshwater anomaly comes from the inner edge of the North Atlantic Current, near  $\sim 50^{\circ}$ N,  $\sim 45^{\circ}$ W, and is advected northward by the overshooting western boundary current. Upon reaching the central Labrador Sea, the fresh anomaly stabilizes the water column, inhibiting convection and reducing the upward doming of the isopycnals. This effect is strong enough in the model to affect the baroclinic structure of the cyclonic circulation in the Labrador Sea. The Labrador Current is weakened, and the flow is eventually diverted to the central Labrador Sea, intensifying the fresh anomaly and further reducing convection. An intense freshwater loss by the ocean is generated by the surface SSS restoration in the central Labrador Sea (Fig. 7b), which however does not overcome the lateral advection of freshwater by the surface currents.

## 8. Summary and discussion

Ocean-only models are usually forced by fluxes based on a prescribed atmosphere, an approach that does not allow for any feedback from the atmosphere and vice versa. Under such forcing, the model thermodynamic adjustment is a direct response to the surface fluxes. In this paper, the response of an OGCM to several surface heat and freshwater flux parameterizations traditionally used in ocean-only models has been investigated using the Miami Isopycnic Coordinate Ocean Model (MI-

COM) configured for the North Atlantic Ocean with medium resolution and with realistic topography and forcing datasets.

First, the model's response to surface heat fluxes computed within the model with the bulk formulas was compared to the response to a Haney-type boundary condition with linearization around SST, and the solutions in both cases were found to be highly similar. To the extent that nonlinearities in the forcing have only secondary importance, the Haney linearization simply makes explicit the restoring to climatology, which is implicit in the bulk formulas. In both approaches, the model is driven toward an equilibrium with a prescribed climatological field, which implies an atmosphere with infinite heat capacity.

With respect to the surface freshwater flux, the model was not found to be significantly sensitive to fluxes that were either entirely prescribed from climatology or combined climatology and modeled SST feedback upon evaporation. This reflects the fact that the largest differences between the surface fluxes in these two cases occur in regions in which the salt balance is dominated by horizontal advection. The SST feedback may become important in long term climate simulations as SST changes at high latitudes lead to in-phase changes in SSS (through evaporation), with competing effects upon convection and upon the strength of the overturning circulation (Hughes and Weaver 1996). With these two surface flux formulations, the modeled SSS diverge sig-

nificantly from observations. Better agreement with observations is observed, as expected, when restoring boundary conditions are used as a proxy for the freshwater flux. This is, however, achieved through the generation of unrealistic surface freshwater fluxes, which differ significantly from the observed fluxes by one or two orders of magnitude. This also implies a meridional freshwater transport, which differs substantially from that inferred from observations, as it adjusts to the unrealistic surface fluxes. With a climatology-based surface flux, the modeled meridional freshwater transport can only converge to observations.

The modeled salinity distribution and meridional freshwater transport will no doubt improve with better observational fields and with error-free models, but alternatives must be sought at the present stage of ocean modeling. Wadley et al. (1996) report on improvements associated with a freshwater flux formulated as a mass flux instead of as a virtual salt flux, but their analysis is restricted to the simulated SST and SSS. If some SSS restoring is necessary to avoid long term drifts, then it can be combined with the flux conditions in order for the model to recover the climatological flux in cases in which it reproduces the climatological SSS. Tziperman and Bryan (1993) discuss such an alternative and suggest, based on error estimates for the surface fields, that the two terms should be weighted differently, with the restoring term accounting for 10% of the forcing. Preliminary results with a high-resolution version of MICOM indicate, however, that a 50% factor may be necessary for a realistic simulation of SSS in the North Atlantic.

The final equilibrium solution under prescribed surface forcing does not reveal anything about how realistic (or unrealistic) the pathways of the simulated transport in the model are. In order to gain some understanding of such pathways, both the meridional freshwater and heat transports were divided into their contributions due to the overturning and to the wind-driven gyres. Analysis of the various components of the transports reveals a picture of the meridional freshwater transport that differs substantially from the one for the heat transport in many aspects; namely, the gyre component is relatively more important for the total freshwater transport than for the total heat transport, which is dominated by the overturning component; the gyre and overturning components of the freshwater transport have opposite signs at midlatitudes; and the decrease in magnitude of the overturning component at low latitudes is more accentuated for freshwater than for heat due to the nonmonotonic decay of salinity with depth associated with the salinity minimum AAIW. Such differences may have important climatic consequences, as they can affect the way in which the overturning circulation will respond to changes in the surface heat and freshwater fluxes.

The combination of surface fluxes, SST, and SSS determines the rate at which water masses are formed and affect the ventilation of the ocean subsurface and deep

layers (Speer and Tziperman 1992). Accordingly, the subduction patterns of the subtropical gyre differ significantly between the freshwater flux and the restoring to observed SSS experiments. While in the former case the increase in SSS (and density) leads to a southwestward migration of the outcropping region accompanied by vertical upward displacement of the isopycnic layers, in the latter case an opposite behavior follows the slight freshening of the surface layer. In the Labrador Sea, convection and production of LSW occur despite the facts that the model cannot resolve the eddy scales of baroclinic instability and that the atmospheric forcing does not contain synoptic scale events (Marshall and Schott 1999). In the present configuration, however, the dominant features associated with LSW formation are the model's ability to simulate the appropriate wintertime mixed layer density and the preconditioning associated with the doming of isopycnals within the cyclonic circulation (Clarke and Gascard 1983). For example, a small decrease in the simulated mixed layer density can reduce the LSW formation, therefore isolating the LSW core from the surface and interrupting its renewal.

Due to numerical (resolution, boundary conditions, . . .) and/or physical (turbulence closure) limitations, no numerical model can perfectly simulate the oceanic advective fields and the associated property distributions. The choices among different surface flux parameterizations, therefore, necessarily involve a trade-off between reproducing the observed climatological fluxes (weak or no oceanic feedback), to the detriment of the representation of the model SST and SSS fields that can diverge from observations, and constraining these fields to closely follow oceanic climatologies (strong, and often unrealistic, restoring boundary conditions), to the detriment of the representation of the surface fluxes. While the physical rationale that exists behind the linearization of the bulk formulas makes the differences between restoring and flux boundary conditions very subtle in the case of heat forcing, with the surface freshwater flux these differences reflect very clearly the different modeling strategies. The model response to these choices is not restricted to the surface fields. Changes in the interior adjustment arise as well, affecting the model's capacity to simulate the production of water masses and the meridional transports of heat and freshwater.

*Acknowledgments.* The authors wish to thank L. Smith for her careful editing of the manuscript. This research was supported by the National Science Foundation through Grant OCE-9531852. AMP was also supported by a fellowship from the Brazilian Research Council (Conselho Nacional de Desenvolvimento Científico e Tecnológico, CNPq).

## REFERENCES

- Barnier, B., L. Siefridt, and P. Marchesio, 1995: Thermal forcing for a global ocean circulation model using a three-year climatology of ECMWF analyses. *J. Mar. Sci.*, **6**, 363–380.
- Baumgartner, A., and E. Reichel, 1975: *The World Water Balance*. Elsevier, 179 pp.
- Bleck, R., and E. Chassignet, 1994: Simulating the oceanic circulation with isopycnic-coordinate models. *The Oceans: Physical-Chemical Dynamics and Human Impact*, S. K. Majundar, E. W. Miller, G. S. Forbes, R. E. Schmalz, and A. A. Panah, Eds., The Pennsylvania Academy of Science, 17–39.
- , C. Rooth, D. Hu, and L. T. Smith, 1992: Salinity-driven thermocline transients in a wind- and thermohaline-forced isopycnic coordinate model of the North Atlantic. *J. Phys. Oceanogr.*, **22**, 1486–1505.
- Böning, C. W., and P. Herrmann, 1994: Annual cycle of poleward heat transport in the ocean: Results from a high resolution modeling of the North and equatorial Atlantic. *J. Phys. Oceanogr.*, **24**, 91–107.
- Bryan, F. O., 1986: High latitude salinity effects and interhemispheric thermohaline circulations. *Nature*, **323**, 301–304.
- , and L. J. Lewis, 1979: A water mass model of the world ocean. *J. Geophys. Res.*, **84**, 2503–2517.
- Bunker, A. F., 1976: Computations of surface energy flux and annual air–sea interaction cycles of the North Atlantic. *Mon. Wea. Rev.*, **104**, 1122–1140.
- Cai, W., 1995: Global present-day ocean climate and its stability under various surface thermohaline forcing conditions derived from Levitus climatology. *Progress in Oceanography*, Vol. 36, Pergamon, 219–247.
- , and P. C. Chu, 1996: Ocean climate drift and interdecadal oscillation due to a change in thermal damping. *J. Climate*, **9**, 2821–2833.
- , R. J. Greatbatch, and S. Zhang, 1995: Interdecadal variability in an ocean model driven by a small, zonal redistribution of surface buoyancy flux. *J. Phys. Oceanogr.*, **25**, 1998–2010.
- Chassignet, E. P., L. T. Smith, R. Bleck, and F. O. Bryan, 1996: A model comparison: Numerical simulations of the North Atlantic oceanic circulation in depth and isopycnic coordinates. *J. Phys. Oceanogr.*, **26**, 1849–1867.
- Chu, P. C., Y. Chen, and S. Lu, 1998: On Haney-type surface thermal boundary conditions for ocean circulation models. *J. Phys. Oceanogr.*, **28**, 890–901.
- Clarke, R. A., and J. C. Gascard, 1983: The formation of Labrador Sea Water. I: The large-scale processes. *J. Phys. Oceanogr.*, **13**, 1764–1788.
- da Silva, A. M., C. C. Young, and S. Levitus, 1994: *Atlas of Surface Marine Data 1994*. Vol. 1: *Algorithms and Procedures*. NOAA Atlas NESDIS 8, U.S. Department of Commerce, NOAA, NESDIS, 83 pp.
- Dickson, R., J. Lazier, J. Meincke, P. Rhines, and J. Swift, 1996: Long-term coordinated changes in the convective activity of the North Atlantic. *Progress in Oceanography*, Vol. 38, Pergamon, 241–295.
- DYNAMO, 1997: Dynamics of North Atlantic Models: Simulation and assimilation with high resolution models. Institut für Meereskunde Tech. Rep. 294, 334 pp.
- Hall, M. M., and H. L. Bryden, 1982: Direct estimates and mechanisms of ocean heat transport. *Deep-Sea Res.*, **29**, 339–359.
- Han, Y. J., 1984: A numerical world ocean general circulation model. Part I: Basic design and barotropic experiment. *Dyn. Atmos. Oceans*, **8**, 107–140.
- Haney, R. L., 1971: Surface thermal boundary conditions for ocean circulation models. *J. Phys. Oceanogr.*, **1**, 241–248.
- Holland, W. R., and F. O. Bryan, 1994: Modeling the wind and thermohaline circulation in the North Atlantic Ocean. *Ocean Processes in Climate Dynamics: Global and Mediterranean Examples*, P. Malanotte-Rizzoli and A. Robinson, Eds., Kluwer Academic, 135–156.
- Hughes, T. M. C., and A. J. Weaver, 1996: Sea surface temperature–evaporation feedback on the ocean’s thermohaline circulation. *J. Phys. Oceanogr.*, **26**, 644–654.
- Isemer, H.-J., and L. Hasse, 1987: *The Bunker Climate Atlas of the North Atlantic*. Vol. 2: *Air–Sea Interactions*. Springer-Verlag, 252 pp.
- Killworth, P. D., D. A. Smeed, and A. J. G. Nurser, 2000: The effects on ocean models of relaxation toward observation at the surface. *J. Phys. Oceanogr.*, **30**, 160–174.
- Large, W., G. Danabasoglu, S. C. Doney, and J. C. McWilliams, 1997: Sensitivity to surface forcing and boundary layer mixing in a global ocean model: Annual mean climatology. *J. Phys. Oceanogr.*, **27**, 2418–2447.
- Lazier, J. R. N., 1973: The renewal of Labrador Sea Water. *Deep-Sea Res.*, **20**, 341–353.
- Levitus, S., 1982: *Climatological Atlas of the World Ocean*. NOAA Prof. Paper No 13, U.S. Govt. Printing Office, 173 pp.
- Macdonald, A. M., and C. Wunsch, 1996: An estimate of global ocean circulation and heat fluxes. *Nature*, **382**, 436–439.
- Marotzke, J., and J. Willebrand, 1991: Multiple equilibria of the thermohaline circulation. *J. Phys. Oceanogr.*, **21**, 1372–1385.
- Marshall, J., and F. Schott, 1999: Open-ocean convection: Observations, theory and models. *Rev. Geophys.*, **37**, 1–64.
- , A. J. G. Nurser, and R. G. Williams, 1993: Inferring the subduction rates and period over the North Atlantic. *J. Phys. Oceanogr.*, **23**, 1315–1329.
- McCann, M. P., A. J. Semtner, and R. M. Chervin, 1994: Transports and budgets of volume, heat and salt from a global eddy-resolving ocean model. *Climate Dyn.*, **10**, 59–80.
- McCartney, M. S., and L. D. Talley, 1982: The subpolar mode water of the North Atlantic Ocean. *J. Phys. Oceanogr.*, **12**, 1169–1188.
- McWilliams, J. C., 1996: Modeling the oceanic general circulation. *Annu. Rev. Fluid Mech.*, **28**, 215–248.
- Moore, A. M., and C. J. C. Reason, 1993: The response of a global ocean general circulation model to climatological surface boundary conditions on temperature and salinity. *J. Phys. Oceanogr.*, **23**, 300–328.
- New, A. L., and R. Bleck, 1995: An isopycnic model study of the North Atlantic. Part II: Interdecadal variability of the subtropical gyre. *J. Phys. Oceanogr.*, **25**, 2700–2714.
- , —, R. Marsh, M. Huddleston, and S. Barnard, 1995: An isopycnic model study of the North Atlantic. Part I: Model experiment. *J. Phys. Oceanogr.*, **25**, 2667–2699.
- Oberhuber, J. M., 1988: *An Atlas Based on the COADS Data Set: The Budget of Heat, Buoyancy and Turbulent Kinetic Energy at the Surface of the Global Ocean*. Max Planck Institute for Meteorology, 202 pp.
- Pavia, A. M., E. P. Chassignet, and A. J. Mariano, 2000: Numerical simulations of the North Atlantic subtropical gyre: Sensitivity to boundary conditions. *Dyn. Atmos. Oceans*, **32**, 209–238.
- Perry, G. D., P. B. Duffy, and N. L. Miller, 1996: An extended data set of river discharges for validation of general circulation models. *J. Geophys. Res.*, **101**, 21 339–21 349.
- Pickart, R. S., 1992: Water mass components of the North Atlantic deep western boundary current. *Deep-Sea Res.*, **39**, 1553–1572.
- Pierce, D. W., 1996: Reducing phase and amplitude errors in restoring boundary conditions. *J. Phys. Oceanogr.*, **26**, 1552–1560.
- Rahmstorf, S., 1996: On the fresh water forcing and transport of the Atlantic thermohaline circulation. *Climate Dyn.*, **12**, 799–811.
- , and J. Willebrand, 1995: The role of temperature feedback in stabilizing the thermohaline circulation. *J. Phys. Oceanogr.*, **25**, 787–805.
- , J. Marotzke, and J. Willebrand, 1996: Stability of the thermohaline circulation. *The Warmwatersphere of the North Atlantic*, W. Krauss, Ed., Borntraeger, 129–157.
- Schmitt, R. W., P. S. Bogden, and C. E. Dorman, 1989: Evaporation minus precipitation and density fluxes of the North Atlantic. *J. Phys. Oceanogr.*, **19**, 1208–1221.
- Schmitz, W. J., and M. S. McCartney, 1993: On the North Atlantic circulation. *Rev. Geophys.*, **31**, 29–49.

- Seager, R., Y. Kushnir, and M. A. Cane, 1995: On heat flux boundary conditions for ocean models. *J. Phys. Oceanogr.*, **25**, 3219–3230.
- Smith, L. T., E. P. Chassignet, and R. Bleck, 2000: The impact of lateral boundary conditions and horizontal resolution on North Atlantic water mass transformations and pathways in an isopycnal coordinate ocean model. *J. Phys. Oceanogr.*, **30**, 137–159.
- Speer, K., and E. Tziperman, 1992: Rates of water mass formation in the North Atlantic. *J. Phys. Oceanogr.*, **22**, 93–104.
- Spencer, R. W., 1993: Global oceanic precipitation from the MSU during the 1979–91 and comparisons to other climatologies. *J. Climate*, **6**, 1301–1326.
- Talley, L. D., and M. S. McCartney, 1982: Distribution and circulation of Labrador Sea Water. *J. Phys. Oceanogr.*, **12**, 1189–1205.
- Tziperman, E., and K. Bryan, 1993: Estimating global air–sea fluxes from surface properties and from climatological flux data using an ocean general circulation model. *J. Geophys. Res.*, **98**, 22 629–22 644.
- , J. R. Toggweiler, Y. Feliks, and K. Bryan, 1994: Instability of the thermohaline circulation with respect to mixed boundary conditions: Is it really a problem for realistic models? *J. Phys. Oceanogr.*, **24**, 217–232.
- Wadley, M. R., G. R. Bigg, D. P. Stevens, and J. A. Johnson, 1996: Sensitivity of the North Atlantic to surface forcing in an ocean general circulation model. *J. Phys. Oceanogr.*, **26**, 1129–1141.
- Weaver, A. J., and E. S. Sarachik, 1991: The role of mixed boundary conditions in numerical models of the ocean climate. *J. Phys. Oceanogr.*, **21**, 1470–1493.
- Wijffels, S. E., R. W. Schmitt, H. L. Bryden, and A. Stigebrandt, 1992: Transport of fresh water in the oceans. *J. Phys. Oceanogr.*, **22**, 155–162.
- Willebrand, J., and Coauthors, 2001: Circulation characteristics in three eddy-permitting models of the North Atlantic. *Progress in Oceanography*, Pergamon, in press.
- Williams, R. G., M. A. Spall, and J. C. Marshall, 1995: Does Stommel’s mixed layer demon work? *J. Phys. Oceanogr.*, **25**, 3089–3102.
- Zhang, S., R. Greatbatch, and C. A. Lin, 1993: A reexamination of the polar halocline catastrophe and implications for coupled ocean–atmosphere models. *J. Phys. Oceanogr.*, **23**, 287–299.